EVALUATION OF POSSIBLE LOCATIONS OF BOTTOM PRESSURE RECORDER FOR THE COLOMBIAN NORTH PACIFIC COAST, USING TSUNAMI TRAVEL TIMES AND TSUNAMI SIMULATIONS

Laura Gonzalez[1]
MEE18708

Supervisor: Shunichi KOSHIMURA[2]
Yushiro FUJII[3]***, Bunichiro SHIBAZAKI**[3]****,**
Saeko KITA[3]****, Hideo FUKUI**[4]******

ABSTRACT

We evaluated the possible locations of Bottom Pressure Recorders (BPR), which provide proper time to issue tsunami warning to the populated areas in the north pacific coast of Colombia. We made a preliminary analysis assuming an arrangement parallel to the subduction trench and then an improvement considering the technical recommendations given by the Pacific Marine Environmental Laboratory regarding the deployment of BPR. With the final arrangement of BPRs, we conducted Tsunami Travel Times (TTT) calculations for far-field events, and tsunami propagation simulation with TUNAMI code. Furthermore, we evaluated the effectiveness of BPR in case of local earthquakes. We classified the possible locations into three groups according to the lead time between tsunami detection on the BPR and the arrival to the first virtual observation point near the most populated areas, as: (1) best, (2) good and (3) not good. We found the best location for the selected arrangement of BPR in latitude 4.909° N, longitude 80.06° W, at the depth of 3,134 meters.

Keywords: Tsunami, Bottom Pressure Recorder, Tsunami Buoy (DART), TTT, TUNAMI.

1. INTRODUCTION

The detection of tsunami in the deep ocean has become very important for tsunami warning centers, as they need to provide early information of the generation of a tsunami. These events may be caused by earthquakes or landslides, and can be detected through a Bottom Pressure Recorder (BPR) anchored on the seafloor, which monitors and reports water column height. The data collected by the BPR is transmitted to the surface buoy through an acoustic modem, and then the surface unit sends this information via satellite communication. After this process, the measurements are transmitted to the tsunami warning centers and to the National Data Buoy Center (NDBC) every three to six hours in regular mode; when the BPR detects a change of 3 cm in the column of water, the event mode is activated, and the information is sent to the surface unit every minute. DIMAR, as National Tsunami Warning Center (NTWC) for Colombia is responsible to provide technical information about the possible impacts of tsunamis for the Colombian coasts and has implemented a network that consists of tide gauges and a tsunami buoy, which is capable of detecting the existence of a tsunami that is approaching the Colombian Pacific coast.

[1] General Maritime Directorate (DIMAR), Colombia.
[2] Professor, International Research Institute of Disaster Science (IRIDeS), Tohoku Univ.
[3] International Institute of Seismology and Earthquake Engineering, Building Research Institute.
[4] National Graduate Institute for Policy Studies.
* Chief examiner, ** Examiner

In 2014, the tsunami buoy was installed in the Pacific Ocean of Colombia, considering the need to give an early warning for the areas in the south of the Pacific coast of Colombia. This study aims to evaluate some possible locations to install a BPR to improve the early warning system for the north regions of the Colombian Pacific coast in case of far-field tsunami events.

2. DATA

In this study, for tsunami simulations we used GEBCO bathymetry grid data with 1 arc-minute resolution for near-field and also for Nicaragua and Peru scenarios. The grid dimension is 1020 x 1200, and the temporal grid size is 3 s. For far field simulations (Kuril and Tonga) it was resampled to 10 arc-minute. The grid dimension is 630 x 1140, and the temporal grid size is 3 s.

For selecting suitable locations of BPRs, we used the nautical chart for the Colombian Pacific Ocean Panama Bay to Cabo San Francisco (Ecuador), which was compiled by the Caribbean Oceanographic and Hydrographic Research Center (CIOH–DIMAR). The scale of the chart is 1:1,200,000 at latitude 04° 47’ 30’’N. We also used the maritime border limits provided by DIMAR.

3. ANALYSIS STAGES

3.1. Preliminary analysis

We assumed a BPR arrangement parallel to the subduction trench to conduct the inverse Tsunami Travel Times (TTT) calculation from populated areas as tsunami source points to the 50 BPRs and Virtual Observation Points (VOP) and evaluate whether this kind of arrangement is effective for the north Pacific coast.

3.2. Improvement of BPR arrangement

We made an improvement on the BPRs arrangement based on considerations made by the Pacific Marine Environmental Laboratory of the National Oceanic and Atmospheric Administration (PMEL-NOAA), to conduct TTT calculations and tsunami simulations considering far-field scenarios to find the locations that gives a proper lead time from the tsunami detection until the arrival to the VOP near the most populated areas in the north Pacific coast of Colombia. Furthermore, we evaluated the effectiveness of the improved BPR arrangement for near-field scenarios.

3.3. TTT calculations

We used TTT software (Wessel, 2009) to calculate tsunami velocity based on an input bathymetry grid and Huygens construction to simulate the propagation of the wavefront from the epicenter to all nodes of the grid as Eq. (1).

$$v\ \ (x,y) = \ \sqrt{g(y)d(x,y)} \qquad (1)$$

where v is propagation speed, g is gravitational acceleration and d is water depths. We selected seven epicenters of far-field events as source points to conduct TTT calculations: Kuril, Aleutians, Papua New Guinea, Tonga, Peru, Nicaragua and Japan.

3.4. Tsunami propagation simulations

For the simulations, we used TUNAMI code modified by Yanagisawa (2019). For the far-field simulations, we used the linear long wave equations in spherical coordinate system as Eqs. (2), (3) and (4):

$$\frac{\partial \eta}{\partial t} + \frac{1}{R\cos\theta}\left[\frac{\partial M}{\partial \lambda} + \frac{\partial}{\partial \theta}(N\cos\theta)\right] = 0 \tag{2}$$

$$\frac{\partial M}{\partial t} + \frac{gh}{R\cos\theta}\frac{\partial \eta}{\partial \lambda} = fN \tag{3},$$

$$\frac{\partial N}{\partial t} + \frac{gh}{R}\frac{\partial \eta}{\partial \theta} = -fM \tag{4}$$

where λ and θ are latitude and longitude respectively, η is water level, M and N are the discharge fluxes in the λ and θ directions, R is the radius of the earth, t is time, g is gravitational acceleration, h is water depth, and f is Coriolis force.

For near-field tsunami propagation simulations, nonlinear long wave equations with Manning bottom friction term were used as Eqs. (5), (6) and (7):

$$\frac{\partial \eta}{\partial t} + \frac{1}{R\cos\theta}\left[\frac{\partial M}{\partial \lambda} + \frac{\partial}{\partial \theta}(N\cos\theta)\right] = 0 \tag{5}$$

$$\frac{\partial M}{\partial t} + \frac{gD}{R\cos\theta}\frac{\partial \eta}{\partial \lambda} + \frac{1}{R\cos\theta\partial\lambda}\frac{\partial}{\partial \lambda}\left(\frac{M^2}{D}\right) + \frac{1}{R\cos\theta}\frac{\partial}{\partial \theta}\left(\cos\theta\frac{MN}{D}\right) + \frac{gn^2}{D^{7/3}}M\sqrt{M^2+N^2} = 0 \tag{6}$$

$$\frac{\partial N}{\partial t} + \frac{gD}{R\cos\theta}\frac{\partial \eta}{\partial \theta} + \frac{1}{R\cos\theta}\frac{\partial}{\partial \theta}\left(\cos\theta\frac{N^2}{D}\right) + \frac{1}{R\cos\theta}\frac{\partial}{\partial \lambda}\left(\frac{MN}{D}\right) + \frac{gn^2}{D^{7/3}}N\sqrt{M^2+N^2} = 0 \tag{7}$$

where n is Manning coefficient, D is the total depth (= η + h).

Table 1. Parameters of source models for the far-field and near-field tsunami simulation.

Scenario	Mw	Longitude (deg)	Latitude (deg)	Length (km)	Width (km)	Strike (deg)	Dip (deg)	Rake (deg)	Slip (m)	Top depth (km)
Far-field										
Nicaragua	9	-86.366	10.286	575.4	144.5	303	12	91	9.5	3
Peru	9	-77.42	-14.20	550	140	329	20	90	11.5	8
Tonga	9	-173.277	-19.972	575.4	144.5	226	22	123	9.5	5
Kuril	9	155.973	47.97	575.4	144.5	215	15	92	9.5	5
Near-field										
North Colombia	7.8	-77.63	6.07	170	85	310	25	40	1.82	3
Central Colombia	7.8	-77.919	4.508	160	80	22	11	116	1.82	3
South Colombia	8.8	-81.00	-0.10	500	180	30	16	120	8.1	5

We used the parameters of the finite fault models described in Table 1 to calculate the initial sea floor deformation in elastic half-space (Okada, 1985). The horizontal displacement effect on the sea surface elevation was also included (Tanioka and Satake, 1996).

For Nicaragua, Tonga and Kuril scenarios we used the scaling law of Papazachos et al. (2004). The parameters of the Peru Earthquake were taken from the source model of Jimenez et al. (2013). Near-field scenarios were determined by considering maximum magnitude calculated according to the length of each segment of the Colombian subduction zone (INGEOMINAS, 2005). The scenario for the south segment was taken from one of the model parameters for the 1906 Esmeraldas earthquake rupture (Mayorga and Sánchez, 2016).

4. RESULTS AND DISCUSSION

4.1. Preliminary analysis

We selected the arrangement of BPR which provided more than 40 minutes with inverse TTT calculations from the populated areas in the north Pacific coast of Colombia as point sources, to the BPRs. The resulting points were the BPRs 31 to 50. Then, we considered some regional scenarios as point sources such as the 2007 Peru earthquake and the 1992 Nicaragua earthquake. From these simulations we evaluated the TTT from these point sources to the VOPs, concluding that these BPRs were effective from the scenarios from the south of Colombia, such as Peru case, but the results from the Nicaragua earthquake showed the same TTT for the first detection in a BPR with the Jurado VOP.

4.2. Improvement of BPR arrangement

We considered the technical recommendations made by PMEL-NOAA (Tang et al., 2008): (1) Seismic noise: When the BPR is located too near to the seismic events that generate tsunamis, seismic noise will be recorded by the BPR as a high-frequency signal and this fluctuation is not related to the tsunami. (2) Water depths and strong currents: The deployment must be done in a zone between 1500 and 6000 meters for the sensor to be able to communicate with the surface unit. (3) Bottom roughness: There might be shadowing in the transmission process due to a presence of a seamount that interrupts the acoustic communication between the BPR with the transducer in the surface buoy. (4) Border limits between the countries.

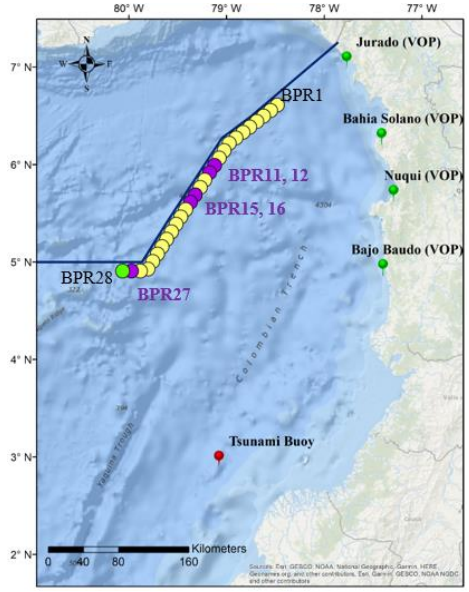

Figure 1. Arrangement of possible locations for BPRs, VOPs and Tsunami Buoy are also shown. The blue line represents the border limits with Panama. The dots represent the BPRs 1 to 28 from north to south. Base map source: NOAA by using GEBCO.

Figure 1 shows the final arrangement of BPRs assumed, VOPs and Tsunami Buoy. The parameters of time from the detection in the BPR to the arrival time of the tsunami to the coastal areas were considered from the procedures of the regional tsunami warning centers: INOCAR in Ecuador and SHOA in Chile. They have determined to have an appropriate response locating their BPRs to a distance from the earthquake generation zone, which in Ecuador case is around 130 kilometers from the coast and in Chile case, from 140 to almost 320 kilometers. They provide their tsunami warning center at least 15- minutes lead time from the detection to the arrival of the tsunami to the coasts.

4.3. TTT calculation

We obtained the TTT from every source point described in Section 3.3 to the possible locations of BPR as shown in Figure 2 and Table 2. In six from the seven scenarios we obtained the first tsunami arrival to BPR 28; in the Peru source, the first detection of the tsunami was made by BPR 26, with just one-minute difference of BPR 28. Also, we compared the TTTs for all the far-field sources with the arrival time to the current BPR installed near Tumaco (Tsunami Buoy in Table 2).

We found that for the far-field cases, the selected location of this study will also improve the detection time in comparison with the current BPR installed, with 20 minutes at least, except the case of the Peru, where the detection was first at the tsunami buoy. With these observations, we were able to determine that the location of BPR 28 is appropriate, considering that at least 15 minutes are given before the arrival to the north Pacific coasts of Colombia.

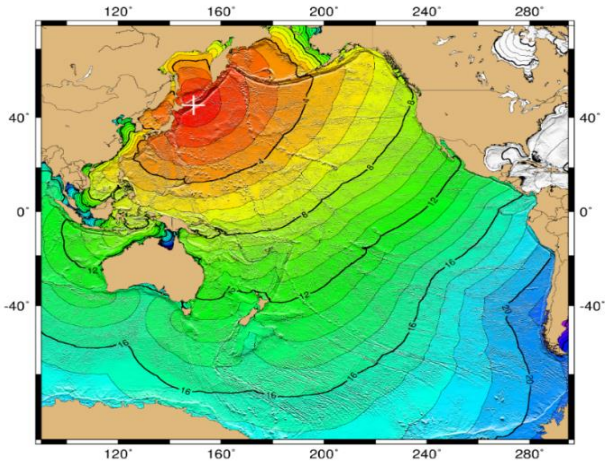

Figure 2. Example of calculations with TTT for Kuril epicenter.

Table 2. Example of results from TTT calculation for Kuril epicenter.

Station	Latitude (deg)	Longitude (deg)	Travel Time	
			Hours	Minutes
BPR28	4.9087	-80.0611	16	43
Jurado (VOP)	7.1027	-77.7666	16	59
Tsunami Buoy	2.986	-79.074	17	6
Nuqui (VOP)	5.7115	-77.268	17	11
Bahia Solano (VOP)	6.2667	-77.3833	17	21
Bajo Baudo (VOP)	4.9526	-77.3713	17	29

The BPR 28 also satisfy the considerations analyzed, because it is not so close to the nearest seismic source, where a BPR can avoid seismic noise. Also, the depths were verified from the nautical chart confirming that the depth of 3,134 meters in the location of the BPR was in the needed range, for the consideration of the communication settings.

4.4. Tsunami propagation simulation

After TTT calculations, we confirmed the obtained results with tsunami simulations with a more realistic tsunami source from the source models in Table 1. In each case we conducted the tsunami propagation simulation as shown in Figure 3 and evaluated tsunami waveforms at the first BPR that register the tsunami, the first VOP near the populated areas and the tsunami buoy as shown in Figure 4. These tsunami simulations confirm the effectiveness of the location of the BPRs in the final arrangement and we were able to evaluate the estimated detection time for a far-field tsunami and also determine that the lead time between the detection on BPR 28 and the arrival to the VOPs was more than fifteen minutes for all the far-field cases we simulated.

4.5. Classification to define position

According to the TTT results from the far-field sources we defined three groups of classification: (1) best (green in Figure 1), for these that will have more than 15 minutes of lead time between the first detection of the BPR and the arrival to the VOP near the populated areas in the north pacific coast of Colombia; (2) good (purple in Figure 1), for 15 minutes; and (3) not good (beige in Figure 1) for less than 15 minutes.

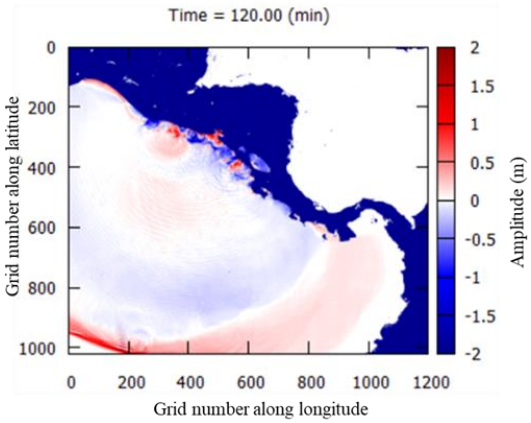

Figure 3. Example of tsunami propagation of the Nicaragua scenario.

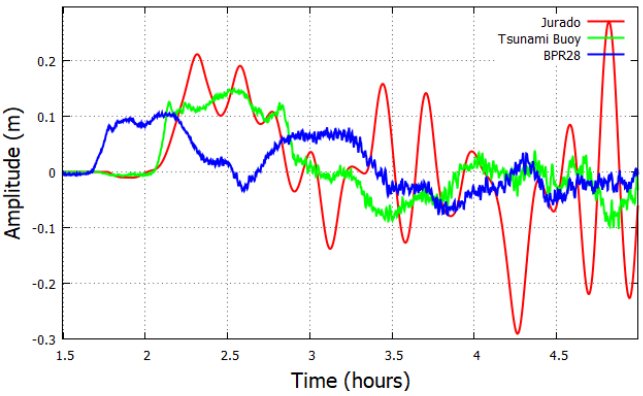

Figure 4. Example of waveforms in Nicaragua scenario. The blue line corresponds to BPR 28. The red and green lines are from Jurado VOP and tsunami buoy, respectively.

5. CONCLUSIONS

For the selected far-field earthquakes, we conducted TTT calculations from point sources and tsunami propagation simulations with a more realistic tsunami source. The results were consistent to conclude that BPR 28 at latitude 4.909° N, longitude 80.06° W, at the depth of 3,134 meters, is the location which provided the suitable response for north area of the Pacific coast of Colombia in most of the cases. We also realized that the location of BPR 28 would provide more time of warning to the central and south areas of the Pacific coast of Colombia.

From the simulations of near-field scenarios, we concluded that for the possible events that occur in the north or central segment, there is no point from the selected locations for BPR in this study, which could give an early detection compared to the actual tsunami arrival time for the populations.

Finally, we defined a classification of the possible locations of BPRs for the north Pacific coast of Colombia as: “best”, “good” and “not good”, according to the resulting times of tsunami arrival to the VOP near the populated areas in the north coast after the detection in the first station within the BPRs.

ACKNOWLEDGEMENTS

I want to express my gratitude to my supervisor Dr. Shunichi Koshimura, Dr. Erick Mas, and my advisor Dr. Yushiro Fujii for their valuable support and suggestion during my study.

REFERENCES

INGEOMINAS, 2005, Instituto Colombiano de Geologia y Mineria, 49 pp.
Jimenez, C., et al., 2013, Journal of Disaster Research, 8(2), 266–273.
Mayorga, E. F., and Sánchez, J. J., 2016, Journal of South American Earth Sciences.
Okada, Y., 1985, Bulletin of the Seismological Society of America, Vol. 75, No. 4, pp. 1135-1154.
Tanioka, Y., and Satake, K., 1996, Geophysical Research Letters, 23(8), 861–864.
Papazachos, et al., 2004, Bulletin of the Geological Society of Greece, XXXVI(April), 1482–1489.
Tang, L., et al., 2008, PMEL-NOAA.
Wessel, P., 2009, Pure and Applied Geophysics, 166(1–2), 301–324.
Yanagisawa, H., 2019, IISEE Lecture note 2018-2019, IISEE/BRI.